\L

J Jacquinot et al

Overview of ITER Physics Deuterium-Tritium Experiments in JET

JOINT EUROPEAN TORUS

JET

Overview of ITER Physics Deuterium-Tririum Experiments in JET

J Jacquinot, V P Bhatnagar, J-G Cordey, L Horton, D F H Start[+],
R Barnsley, P Breger, J Christiansen, S Clement, S Davies,
J Ehrenberg, L G Eriksson, G Fishpool, M Gadeberg,
P Harbour, H Jackel, K Lawson, J Lingertat, C Lowry, C Maggi,
G Matthews, R Monk, D O'Brien, E Righi[1], G Saibene,
R Sartori, B Schunke, A C C Sips, M Stamp, D Stork,
J Strachan[2], A Tanga, K Thomsen and the JET Team..

JET Joint Undertaking, Abingdon, Oxfordshire, OX14 3EA,
[1]The NET Team, Max-Planck Instuut für Plasmaphysik, Garching 85748, Germany.
[2] Plasma Physics Laboratory, Princeton University, Princeton, NJ 08543 USA.
[+] Passed away

ABSTRACT

An overview of JET experimental results in DT plasmas directly relevant to ITER modes of operation are presented. Experiments in D:T mixtures varying from 100:0 to 10:90 and those carried out in hydrogen plasmas, show that the H-mode threshold power has approximately an inverse isotopic mass dependence. Matching some of the key dimensionless parameters to the ITER values, the ITER-similarity experiments with ITER shape and safety factor (q) show that the global energy confinement time is practically independent of isotopic mass ($\sim A^{0.03\pm0.08}$) where A is the atomic mass of the hydrogenic species. Subtracting the edge pedestal energy (which scales as $\sim A^{0.57\pm0.2}$) from the total stored energy leads to a $\sim A^{-0.17\pm0.1}$ dependence of confinement in the plasma core, very similar to that expected from the gyro-Bohm transport ($\sim A^{-0.2}$) model. The observed scaling of the edge pedestal energy is consistent with a model in which the edge pressure gradient saturates at the ballooning limit over a region of width that scales as the ion poloidal Larmor radius governed by the average energy of the fast-ions in the edge. The steady state total stored energy for a given input power in both ion cyclotron resonance heated (ICRH) and NBI discharges is the same despite the lower edge pedestal in the ICRH case which is compensated by a more peaked power deposition profiles in ICRH. ELM frequency is smaller with NBI; it decreases with isotopic mass both in NBI and ICRH discharges. A steady-state, type I ELMy H-mode discharge with ITER shape and q at 3.8 T/3.8 MA with an input power of 22 MW, produced a Q≈0.18 for 3.5 s and extrapolates well to ignition with ITER parameters. Here, Q is the ratio of fusion output power to input power. The thermal ELMy H-mode confinement both in deuterium and tritium gas fueled plasmas decreases significantly when the plasma density exceeds 0.75 of the Greenwald (n_{GW}) limit and the maximum density achieved is $0.85 n_{GW}$. In L-mode, the density limit decreases with increasing isotopic mass roughly in accordance with code predictions. ITER reference ICRH scenarios have been evaluated. Second harmonic heating of tritium at densities available in JET produces strong tails and heats electrons predominantly as expected. He3-minority in 50:50 D:T and tritium dominated plasmas showed strong bulk ion heating leading to ion temperatures up to 13 keV with ICRH alone. Deuterium minority ion cyclotron heating in tritium plasmas at a power level of 6 MW produced a steady-state record values of Q≈0.22 for more than 2.5s.

1. INTRODUCTION

The present campaign of JET which extends to the end of 1999 has two main physics objectives: (i) to contribute to the realization of a mature divertor concept for ITER [1] and (ii) to provide the physics support for ITER. The most significant contributions to the second objective have been made with the full fledged operation (DTE1 experiments) of JET in DT plasmas. The experiments in DTE1 [2] can be divided into two areas: (i) ITER modes of operation and (ii) high fusion performance. Results obtained in the second area are discussed in a companion

paper [3]. Here, we concentrate on the results obtained in the first area which is crucial for a more accurate prediction of ITER performance and ignition margin. Experiments performed in this area are (a) the isotope scaling of H-mode threshold power, energy confinement, edge localized modes (ELMs) and edge pedestal together with an insight into core and edge transport physics, (b) steady-state ELMy H-mode experiments providing a sustained high fusion power output and data on confinement at high density including the density limits in L and H-mode and (c) ion cyclotron resonance heating (ICRH) experiments including the demonstration of ITER reference scenarios of second harmonic heating, D-minority heating in tritium plasmas and benchmarking of ICRH codes for ITER applications. The main constraint limiting the extent of experiments in the area of ITER modes of operation was the neutron budget which was set at 8.5×10^{19} neutrons.

JET has considerable flexibility that allows exploration of the proposed ITER modes of operation. It can match ITER geometry, safety factor q and most of the key physics dimensionless parameters such as β and ν^*. The largest deviation is in the normalized Larmor radius ρ^* which is a factor of 3 to 5 higher in JET than in ITER. The parameter ρ^* is a key parameter in the prediction of ITER performance and it has been varied systematically in these experiments in order to provide the basis for extrapolation to ITER. Here, ρ^* ($\equiv \rho_i/a$), ν^* ($\equiv \nu_e a/\nu_{th}$) and β ($\equiv 2\mu_0 <p>/B_\varphi^2$) where ρ_i is the ion Larmor radius, a is the minor radius in the mid-plane, ν_e is the electron-ion collision frequency, ν_{th} is the ion thermal velocity, <p> is the average plasma pressure and B_φ is the toroidal field.

In view of the limited neutron budget during the DTE1 campaign, automatic feedback real-time control systems have been implemented so that if the desired performance or a desired plasma parameter is not achieved at the expected time during a discharge, the plasma shot is terminated with a soft landing. Also, various combinations of plasma parameters can be maintained at a programmed level by a system controlling, in real time, a number of auxiliaries such as neutral beam injection (NBI), ICRH and lower hybrid current drive (LHCD) power thus improving reliability of discharges. Using digital real-time control techniques, ICRH and/or NBI power delivered to the plasma can be controlled with precision.

The 20 g of tritium available on-site permitted a significant number of D/T shots during a period typically lasting 3-4 days. The exhaust gases were collected and reprocessed (usually in 3-4 days) by the on-site closed-circuit Active Gas Handling System (AGHS) [4] for subsequent experiments. The tritium usage during DTE1 experiments at JET is illustrated in Fig. 1 where integrated values of tritium supplied by the AGHS plant for JET DT experiments is plotted as a function of time starting 19 May to 17 November 1997. The tritium gas was either injected directly to the torus via a gas valve or supplied to the NB box which then injected a small fraction of it to the torus via the neutral energetic tritium beams. The remaining gas was trapped by the NB cryo-pumps which was retrieved by regeneration and then reprocessed by the AGHS plant for reuse. It can be seen that in all, about 100 g of tritium was injected and reused out of
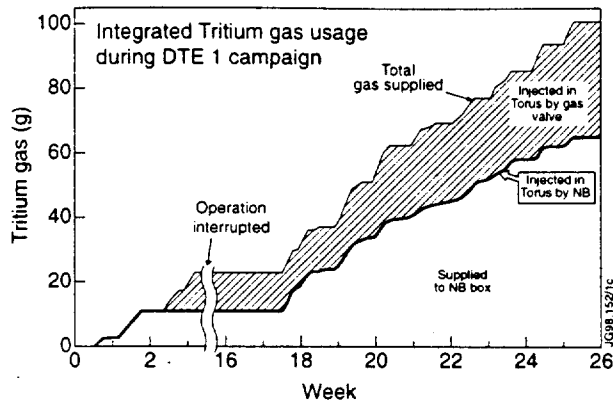
FIG. 1. Integrated values of tritium gas supplied and used in the JET DTE1 experiments as a function of time. The experiments began on 19 May and ended on 17 November 1997. The gas supplied to the tritium NB box, to the torus directly and that injected by the NB box have been identified.

which only about 1mg was consumed in the fusion reactions. The staircase behavior is related to the weekly usage and reprocessing of tritium with a significant gap of time of non-usage where a leak developed in a JET system was being repaired. Tritium concentrations in the plasma could be well controlled by loading the vessel walls with tritium in Ohmic or low power ICRH discharges. More than 80% of tritium concentration in Ohmic plasmas could be obtained with about ten 100% tritium gas fueled discharges. With significant supplementary heating (>10MW), additional tritium loading discharges were required to maintain a high tritium concentration. During the DTE1 campaign, a total of 220 discharges with $n_T/(n_D+n_T)>0.4$ were made. After this campaign, tritium cleaning experiments removed 5.3 g of tritium but a significant amount (6.2 g) remained trapped in the plasma facing components and in the divertor structure. Most of the trapped tritium is expected to be retrieved from carbon tiles and carbon flakes during the divertor tile exchange being carried for the next phase of the JET experimental programme.

In section 2, we briefly outline the experimental set-up used in the DTE1 experiments. Sections 3 and 4 deal with the isotope scaling of H-mode power threshold and energy confinement, respectively. The steady-state ELMy H-modes are discussed in section 5 whereas ELMs and the edge pedestal are dealt with in section 6. In section 7, we consider the trace tritium particle transport and the L and H-mode density limit issues are addressed in section 8. Experimental results of ITER reference ICRH scenarios are presented in section 9 and finally, the discussion and conclusions of the paper are contained in section 10.

2. EXPERIMENTAL SET-UP

A poloidal cross section of JET [5,6] showing the four divertor coils, carbon fibre composite (CFC) target plates held by a water cooled structure, cryopump, ICRH antenna and poloidal limiter inside the vacuum vessel is given in Fig. 2 (a). JET has a single null (bottom X-point) divertor configuration similar to ITER. The DTE1 experiments were carried out with the so-called MkIIaP divertor [7] as shown. Plasma equilibrium code reconstructed flux surfaces together with the separatrix for a 3.4 T/4.5 MA discharge are as illustrated. The JET ICRH [8] system couples up to 16 MW of power via four antennas distributed around the torus (see Fig. 2(b)). The ICRH antennas are equipped with Faraday shields made out of beryllium. Each antenna has four straps which can be phased independently. The system has been operated at
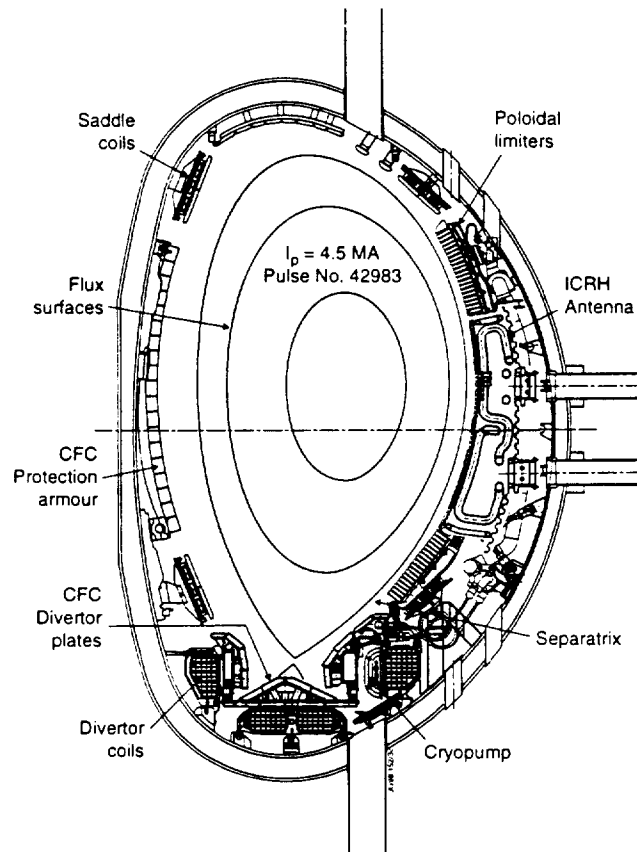
FIG. 2 (a). *A poloidal cross section of the D-shaped JET showing the four divertor coils, MkIIaP divertor target plates, cryopump, ICRH antenna, poloidal limiter and saddle coils inside the vacuum vaessel. Plasma flux surfaces together with the separatrix of a 4.5 MA discharge are also illustrated.*
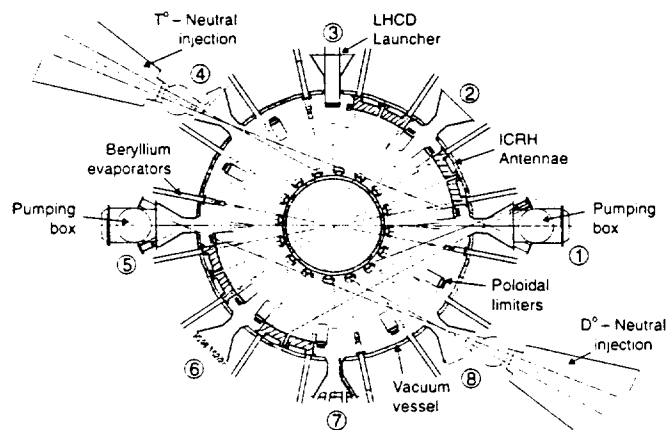

FIG. 2 (b). *A plan view of the JET tokamak identifying the locations of tritium and deuterium neutral beam injection boxes. Also the distribution of ICRH antennae and the LHCD launcher have been marked.*

4

various frequencies (23-56 MHz) over the full bandwidth of the system. A number of poloidal limiters in CFC protect each antenna unit from the two sides. The NBI system [9] consists of two beam boxes (see Fig. 2(b)). One of them has been used to deliver up to 100% tritium beams injecting about 11 MW of tritium beam power at 155 kV for up to 5 s. The other box is used for deuterium beam injection delivering up to 12 MW at 140 kV. The average beam power delivered by the 16 sources is varied continuously using the feedback control pulse-width modulation technique. The LHCD system [10] which includes a cryopump is capable of delivering up to 7MW of power. Glow discharge is used for wall conditioning after a vent and beryllium evaporation is carried out when needed for gettering purposes (less than once a day). The tokamak operation is carried out with vessel walls at 300°C.

The standard JET diagnostics for electron density (n_e), electron temperature (T_e), ion temperature (T_i), effective charge (Z_{eff}) have been discussed elsewhere [12]. For tritium compatibility and safety, certain modifications were made to the installed diagnostics. These include double containment vacuum feed-throughs with 500 mBar neon gas in the interspaces, exhaust from diagnostics vacuum systems sent to AGHS plant when necessary, extra neutron shielding, radiation hardened video cameras and heated optical fibres to recover from radiation damage. The most notable new diagnostics in DTE1 were the 14 MeV neutron tomography and the measurements of the tritium concentration in the core and edge of the plasma as well as in gaseous exhaust after a discharge using residual gas analysis (RGA) and ion chamber measurements. The tritium concentration in the core was estimated from neutron emission rates and active Balmer-α charge exchange measurements. In the plasma region 20-40cm inside the separatrix, the tritium concentration was derived from neutral particle analysis (NPA) by electrostatic deflection and time of flight techniques. Near the separatrix, Balmer emission spectroscopy was used. Below divertor tiles, Balmer emission from Penning discharge gauges was implemented [13].

3. H-MODE POWER THRESHOLD

The design of ITER relies on operating in the H-mode confinement regime to achieve ignition. Experimental data indicate that the H-mode operation requires a threshold power. Although a plausible conceptual picture of H-mode suppression of edge turbulence due to velocity shear layers exists [14], a theoretical scaling of the threshold power is not available. Consequently, an empirical approach is generally used. It is assumed that the power threshold is determined by the total heat flux crossing through the separatrix. Using dimensional analysis, the following form of the H-mode threshold power

$$P_{th} = 0.45 \, n_e^{0.75} \, B_\varphi R^2 \tag{1}$$

can be deduced where power coefficients of the engineering parameters in the above equation are constrained to make the relation dimensionally correct [15]. This equation fits with the data from a number of tokamaks world-wide [16] albeit with a significant scatter. Here, P_{th} represents the threshold power (see below) for a transition from L to a dithering H mode, n_e is the line-averaged electron density (in $10^{20}\,\mathrm{m}^{-3}$), B_φ is the toroidal magnetic field on-axis and R is the tokamak major radius. The above expression gives explicit dependence on n_e, B_φ and R but the threshold power is also found to depend on the direction of the ion ∇B drift, vessel wall conditioning, plasma-limiter distance, edge current density and on the isotopic mass. Here, with the JET data available in deuterium-tritium mixtures, we emphasize the isotope mass scaling of the threshold power for a more accurate assessment of the power required in ITER to access the H-mode in DT plasmas. In order to extend the mass range, experiments were also performed in hydrogen plasmas. Dedicated experiments have been carried out in JET with ICRH and NBI heating using slow ramps in power to determine the threshold power accurately. Plasma discharges with ITER shape and q at magnetic fields ranging between 1 and 3.8 T and densities in the range of 2 to 5 x 10 ^{19} m^{-3} have been used.

For a set of parameters (B_φ=2.6T and I_p = 2.6 MA), in Fig.3, we show time traces of $H_\alpha/D_\alpha/T_\alpha$ and ICRH/NBI power in four shots with different gases: (i) H-plasma heated with H^0-NBI. (ii)-(iv) in three different D/T gas mixtures of 100:0, 50:50 and 10:90 respectively and heated with ICRH in H-minority scheme. As indicated in the figure, H-mode occurs (appearance of threshold or type III ELMs [17] in the D_α-signal) at the highest power in H-plasmas and at the lowest power in T-plasmas.

As the transition to H-mode is understood to be essentially an edge phenomenon, the power flowing outwards from the center and crossing the separatrix is believed to be of importance. Therefore, we take P_{th} to be the power crossing the separatrix:

FIG. 3. D_α-signal and input power plotted as a function of time in four shots with different gas mixtures: hydrogen, deuterium, 50:50 D:T and 10:90 DT. Same input power (6.7 MW) with a slow ramp was used to identify the onset of H-mode at the first appearance of ELMs as indicated. Threshold power decreases with increasing isotopic mass.

$$P_{SEP} = P_{IN} - dW/dt - P_{RAD}^{bulk}$$

where P_{IN} is the total input power, W is the stored energy in plasma and P_{RAD}^{bulk} is the radiated power from the bulk of the plasma. A regression analysis has been carried out on the above
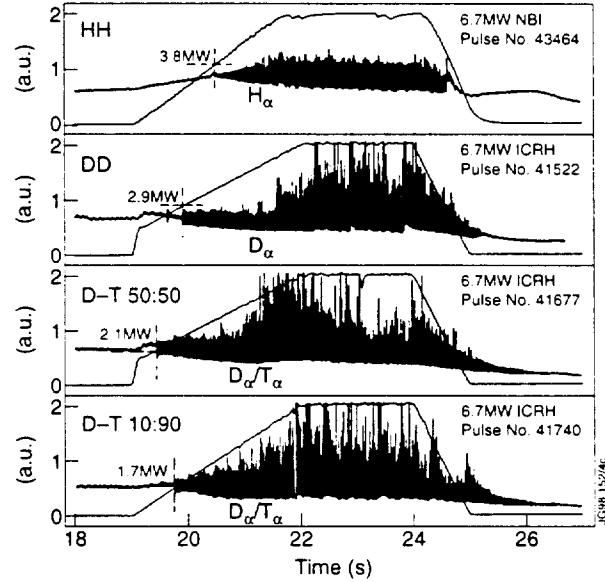
6

defined loss power (P_{SEP}) at H-mode threshold for the JET data which includes a range of plasma current and magnetic fields in hydrogen and in DT mixtures ranging form 100:0 to 10:90. In this analysis, in addition to using the same scaling parameters n_e, B_j and R as in Eq. 1, we have also included the isotopic mass (A) dependence. But, no regression was done on R as in the JET data, the value of R does not change significantly. The power exponent of R has been adjusted such that Eq. 2 satisfies the constraint [15] to make the expression dimensionally correct. The result of this regression is shown in Fig. 4 and the power threshold scaling expression found is given by:

$$P_{th} \text{ (scaling)} = 0.97 \; n_e^{1.17} \; B_\varphi^{0.71} \; R^{2.48} \; A^{-1.04} \tag{2}$$

The threshold power data shows roughly an inverse mass dependence. This predicts a significant reduction in the power needed for accessing the H-mode in ITER and increases the operational flexibility of ITER
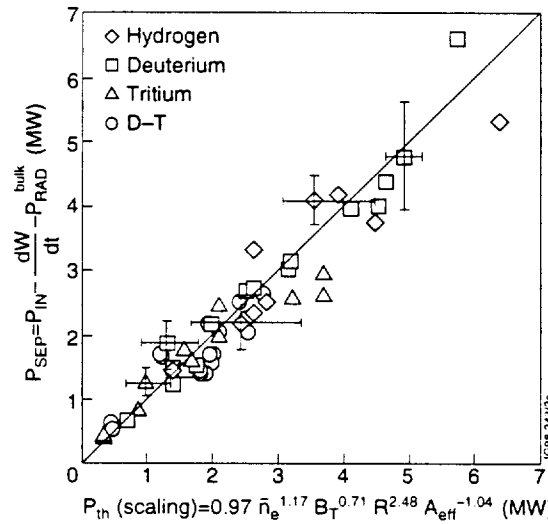

FIG. 4. The power crossing the separatrix (P_{SEP}) representing the L-H threshold power of JET discharges in hydrogen, deuterium, 50:50 D:T and 10:90 D:T mixtures is plotted against a scaling obtained by a regression analysis in which the A^{-1} mass dependence has been added to the ITER scaling [15]. This regression of JET data indicates an approximate inverse mass dependence of the threshold power. No regression has been done on R. Here, W is the plasma stored energy and P_{RAD}^{bulk} is the radiated power from the plasma bulk.

4. ENERGY CONFINEMENT

With a view to predicting the energy confinement time in ITER more accurately, JET has carried out dedicated experiments, the so-called ρ^*-scaling experiments, in which carefully constructed ITER similarity pulses are used to assess ITER relevant ELMy H-mode energy confinement [19]. Key physics dimensionless parameters such as β, v^* and q are fixed at their ITER value save the dimensionless Larmor radius $\rho^* (\equiv \rho/a)$ The JET machine is the one closest to ITER

with the smallest ρ^*-values within a factor of 5 from that of ITER. This parameter is varied in JET to determine the ρ^*-scaling of confinement and then extrapolated to ITER. Data from other machines has also been used to extend the range of ρ^* [19]. Here, with the availability of JET data in DT plasmas, we emphasize the effect of the isotopic mass on confinement scaling.

Due to the influence of isotope mass on H-mode threshold power and ELM behaviour, it is not always possible to obtain the same density for the same input power in all conditions of operation. Nevertheless, it was possible to match the density and power in a number of cases and one such example is shown in Fig. 5 at B_ϕ=1T and I_p=1MA where I_p refers to the discharge current. Here, two discharges one with D^0-beam in D-plasma and the other with T^0-beam in T-plasma are shown for illustration.

FIG. 5. A comparison of two similar discharges at B_t =1T and I_p= 1MA with $D^\circ \to D$ and $T^\circ \to D:T$ (10:90%) at equal stored energy (W_{DIA}), volume averaged density ($<n_e>$) and NBI heating power (P_{NBI}). D_α and T_α-signals show that in the $D^\circ \to D$ discharge, the frequency of type I ELMs is higher by a factor of 1.75.

We note that the stored energies measured by a diamagnetic loop are quite similar both in D and T-discharges when the input power and the densities are the same indicating no isotopic mass dependence on confinement. However, note that the frequency of type I ELMs is lower (a factor of about 0.6) in tritium as compared to deuterium plasma (see also Fig. 11).

A comparison of JET ELM-free H-mode confinement data in DT plasmas with ITERH93-P scaling [20] shows that its $A^{0.4}$ dependence is clearly too strong and does not fit the JET DT data. It is however not far from fitting the gyro-Bohm physics form [21] where the mass dependence is $A^{-0.2}$ as shown in Ref. [22]. Turning to the steady-state ELMy H-modes, a data set with matched power and density in H, D, DT and T-plasmas has been assembled. A regression analysis which is presented in Fig. 6 shows that, in fact, the mass dependence is close to zero ($\sim A^{+0.03\pm0.08}$). Further analysis reveals that in neutral beam injection (NBI) heated discharges, subtracting the edge pedestal energy (which scales as $\sim A^{0.57\pm0.2}$) from the total stored energy leads to a $\sim A^{-0.17\pm0.1}$ dependence of confinement in the plasma core, very similar to that expected from the gyro-Bohm transport model. Note that the observed scaling of the edge pedestal energy is consistent with a model in which the edge pressure gradient saturates at the ballooning limit over a region of width that scales as the ion poloidal Larmor radius (see section 6). Thus the net effect of the isotopic mass is negligible in the global energy confinement time [23] as the two effects roughly cancel each other.
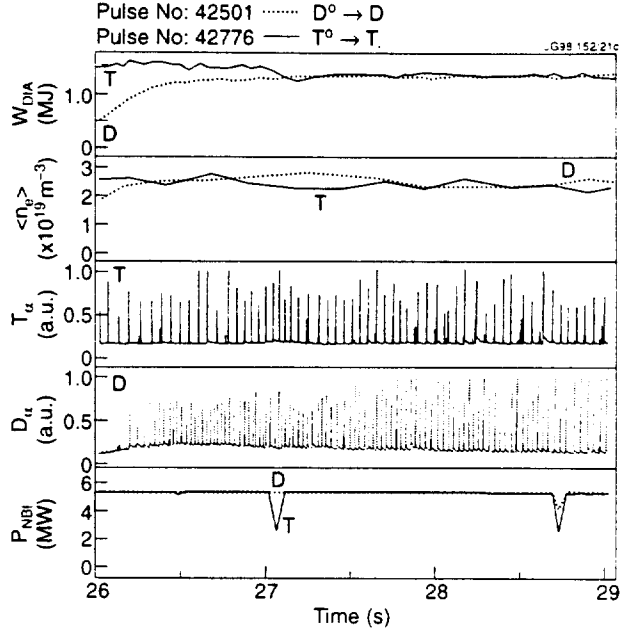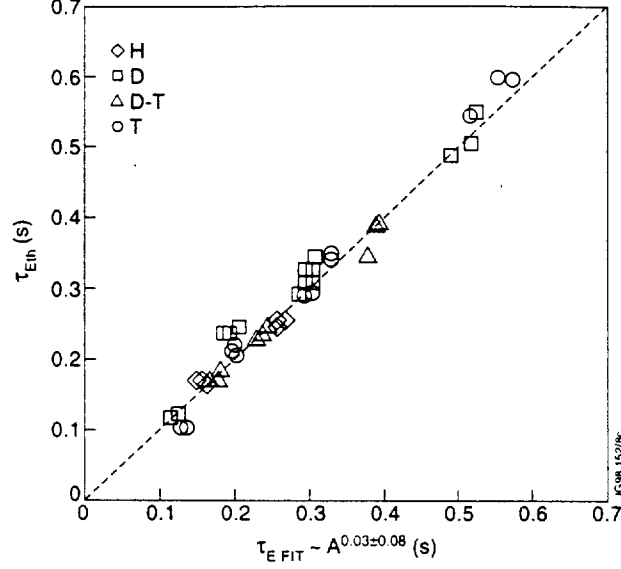
8

FIG. 6. Thermal energy confinement time data of JET ELMy H-mode NBI and ICRH discharges in hydrogen, deuterium, 50:50 D:T and 10:90 D:T mixtures are plotted against a fit where all power coefficients are the same as in the physics form of the gyro-Bohm scaling (ITERH-97Py) except that of mass. $\tau_{E\,FIT} = 1.17\ \tau_E * A^{0.03\pm0.08}$. The good fit shows that confinement is roughly independent of the isotopic mass. The scaling ITERH-97Py [19] is given by $\sim0.029\ \tau_E * A^{0.2}$ where $\tau_E * = I^{0.9}\ B^{0.2}\ P^{-0.66}\ n^{0.4}\ R^{2.03}\ \varepsilon^{0.19}\ \kappa^{0.92}$.

FIG. 7 (a). Thermal energy confinement time data of JET L-mode discharges in hydrogen, deuterium, and D/T mixtures are plotted against the ITER L-mode scaling $\tau_{EITERL96} \sim I^{0.96}\ B^{0.03}\ \kappa^{0.64}\ R^{1.83}\ (R/a)^{0.06}\ ne^{0.4}\ P^{-0.73}\ A^{0.2}$ [24].
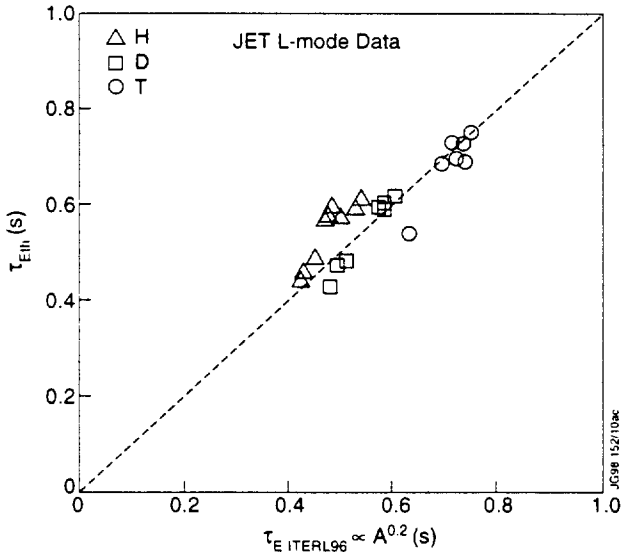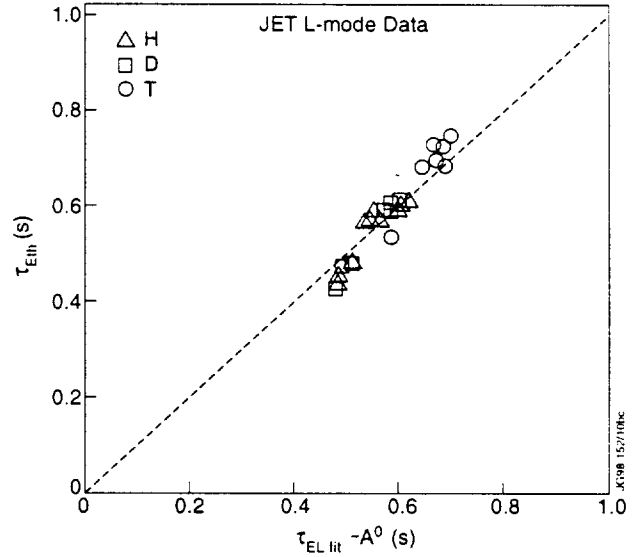
FIG. 7 (b). Thermal energy confinement time data of JET L-mode discharges in hydrogen, deuterium, and D/T mixtures are plotted against the ITER L-mode scaling as in Fig. 7 (a) except the mass dependence i.e. $\tau_{EL\,FIT} = C\ \tau_{EL} *.\ A^0$ where $\tau_{EL} * = \tau_{EITERL96}A^{-0.2}$ and C is a constant.

We have also studied the L-mode confinement in similar JET divertor discharges in H, D and DT mixtures. The L-mode data has been plotted against the ITERL96-P scaling [24] which has an $A^{0.2}$ dependence on the isotope mass. We present plots of thermal energy confinement time against the above L-mode scaling with and without the mass dependence in Fig. 7 (a) and

9

(b) respectively. The fit of JET experimental data shows that it does not depend on the isotopic mass. This is in contrast to the TFTR L-mode DT shots which showed $A^{0.3-0.5}$ dependence [25]. The reason for this difference is not clear. However, we point out that to remain in L-mode in X-point discharges, the data in Fig. 7 have very low auxiliary heating power especially in the tritium dominated discharges as compared to TFTR limiter L-mode discharges. Thus JET data is close to the Ohmic regime which in the case of TFTR also showed weak $(A^{0-0.3})$ dependence on isotope mass.

5. STEADY STATE OPERATION IN ELMY H-MODES

The best fusion performance in JET DT plasmas has been obtained in enhanced confinement ELM-free hot-ion H-modes though only transiently [3]. In addition, high performance in nearly steady-state ELMy H-mode discharges has been obtained under ITER-like conditions with the key physics dimensionless parameters such as β, ν^* and q being fixed close to their ITER value. Furthermore, central electron and ion temperatures were roughly equal. However, due to the lack of input power, in some discharges, β-values can fall short of the one required in ITER.

The time evolution of a 3.8 T / 3.8 MA high performance steady-state ELMy H-mode discharge in a 50:50 DT plasma with a total input power of 22 MW (predominantly NBI-power) is illustrated in Fig. 8. The discharge has type I ELMs throughout and the stored energy is practically stationary for 3.5 s which is about 8 energy confinement times. The duration of the discharge is only limited by the neutron economy or the NBI duration. Fusion power output which reached a steady-state value of more than 4MW is also shown. Using a conservative definition of fusion Q, as the ratio of fusion output power to total input power, its value is 0.18 over 3.5 s of the discharge. Integrated over the entire pulse, the fusion energy reached a value of 22 MJ which is a world record. The central line averaged density is about 7×10^{19} m^{-3} which droops a little towards the end of the high performance phase of the discharge. At such a high density, due to the short electron-ion equilibration time, the electron and ion temperatures are roughly
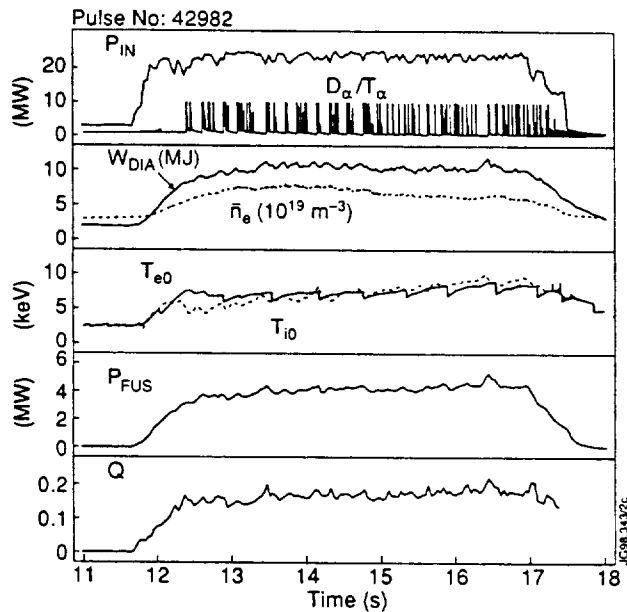

FIG. 8. Time traces of a near steady-state high performance JET discharge at 3.8T/3.8MA in 50:50 D:T mixture with an input power (P_{in}) of 24 MW. Diamagnetic stored energy (W_{DIA}) reached 10.5 MJ, fusion power output (P_{FUS}) and total Q ($\equiv P_{FUS}/P_{in}$) are 4.1 MW 0.18 respectively. Other signals are: D_α/T_α-emission showing ELMs, central line averaged plasma density (n_e), central electron (T_{e0}) and ion (T_{i0}) temperatures.

10

equal at about 8.5 keV. Another ELMy H-mode steady-state discharge [26] at a lower value of $q_{95}= 2.8$ (3.8 T/4.5 MA) was found to have no degradation in confinement with respect to ITERH-97P-scaling. These results at lower q in DT-plasmas, which are of significant interest for ITER, are further supported by the ITER similarity experiments in deuterium plasmas [26].

A high performance steady state discharge (3.7 T/3.7 MA) was also obtained by ICRF heating alone [27] with D-minority heating in a tritium plasma (9:91 D:T mixture). Despite the DT mixture being far away from 50:50, a fusion power output of 1.6 MW was obtained with an input ICRH ($f=f_{CD}=28$ MHz) power of 6 MW only as shown in Fig. 9. In this discharge, the plasma density and the minority ion concentration was such that the average deuterium tail energy was about 120 keV

FIG. 9. Time traces of a near steady-state JET discharge at 3.8T/3.8MA in 9:91 D:T mixture heated by ICRH in D-minority in tritium with an input power of 6 MW. Fusion power output is 1.6 MW making a record Q=0.22 for a duration of more than 2.5 s. Here, H97 represents the ITERH97-Py H-mode confinement factor which is above the value required by ITER.

(close to the peak of DT fusion cross section). In this discharge, the neutrons thus produced are predominantly of non-thermal origin. The steady-state (for about 2.7 s) Q value is about 0.22 (a record value in steady-state conditions) whereas the bulk ion and electron temperatures are both at 7 keV. The neutron yield could be well reproduced by the PION code and confirms the non-thermal origin of these neutrons [28]. The PION code uses a sawtooth redistribution model but otherwise has no free parameters.

6. ELMS AND EDGE PEDESTAL

Edge localised modes (ELMs) are MHD instabilities which occur during H-modes and produce bursts of energy and particles that are ejected through the separatrix to the scrape-off layer and ultimately end up predominantly in the divertor. For steady-state, it is desirable to operate ITER in ELMy H-mode as this regime can provide sufficiently high confinement quality factor and may prevent the uncontrolled build up of density, impurity and helium ash. The H-mode behaviour is initiated at the plasma edge where a confinement barrier is formed. The reduced transport then propagates to the plasma core. The edge pedestal energy contributes significantly to the stored energy.

Assuming that the critical edge electron pressure ∇p_e^{crit}, just before the crash of an ELM is limited by the ballooning instability, we obtain the scaling expression: $\nabla p_e^{crit} \propto I_p^2 S$ [29] where
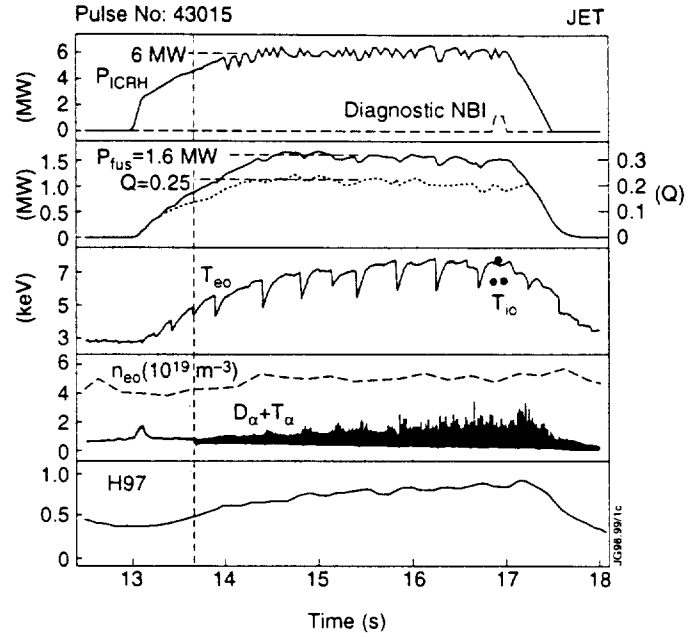
I_p is the plasma current and S is the magnetic shear at the edge. Approximating ∇p_e^{crit} by p_e^{crit} / Δ, we can write

$$p_e^{crit} \propto I_p^2 \, S \, \Delta \propto \rho_i \propto (AE)^{1/2} \qquad (3)$$

where E is the averaged energy of the ions in the edge and Δ is the width of the edge transport barrier which is assumed to be governed by the ion Larmor radius ρ_i.

We have attempted to apply these guiding principles to the understanding of the behaviour of ELMy H-mode discharges heated by NBI and ICRH in H, D, and DT plasmas. Edge electron pressures for a series of shots heated by NBI and ICRH are presented in Fig. 10 as a function of isotope mass. Note that for practical reasons, the edge pressure is computed at a major radius of 3.75m (normalized minor radius of ~0.9) at the location of a density measuring interferometer chord. The broken line ($\sim A^{1/2}$) in Fig. 10 has been drawn normalized to an NBI deuterium point for comparison. The NBI experimental data increases somewhat more strongly than $A^{1/2}$ whereas the electron pressure for the ICRH data is much smaller and is practically independent of the isotopic mass. Clearly the scaling derived from Eq. 3 does not represent adequately the observations. An analysis presented in Ref. 29, suggests that the

FIG. 10. Maximum edge electron pressure (@ R=3.75m in JET) is plotted as a function of isotopic mass of JET plasma in experiments carried out in different gas mixtures: hydrogen, deuterium, 50:50 D:T and 10:90 DT both in ICRH and NBI heated discharges. For comparison, the values have been normalized by the parameters given in Eq. 3. The broken line, representing the $A^{0.5}$ dependence, is drawn for comparison and has been normalized to an NBI point in deuterium.

transport barrier width Δ is not determined by the average ion energy but by the energy of the fast-ions residing in the edge. In NBI heating, a certain fraction of the neutral beam energy is carried in the 1/2 and 1/3 components which deposit fast ions at the edge. The operating voltages (or energy of the beams) increases as we change from H° to D° and T°-beams which contributes to an additional increase in pedestal width with the isotopic mass.

In the case of ICRH, there is little direct fast-ion deposition in the edge but due to large orbits, minority species fast ion tails may indirectly contribute to the edge energy. However, this contribution to the edge energy is much smaller than in the case of NBI. Despite the lower edge pedestal in the ICRH, the steady-state total stored energy in both ICRH and NBI cases is the same. This is due to the fact that the power deposition profile in the ICRH is more peaked than in the NBI case [29]. A TRANSP analysis carried out on two comparable ICRH and NBI discharges confirms the above finding. For the three ICRH shots presented in Fig. 10, the same
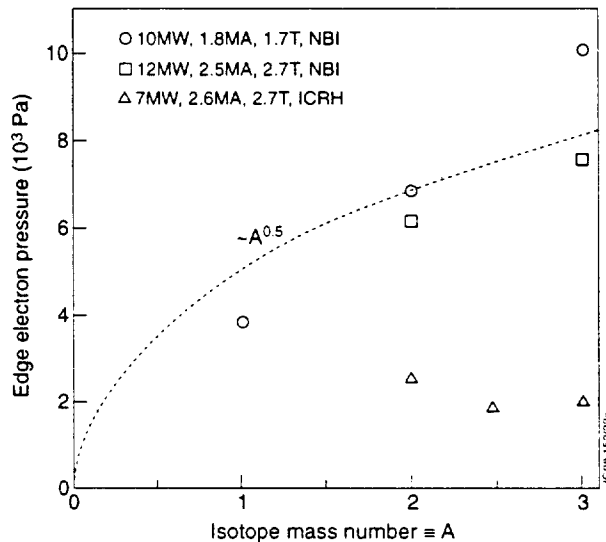
minority species hydrogen was heated in D, DT and T-plasmas. If the energy of fast ions in the edge determines the edge pedestal, no marked mass dependence is expected even though the majority gas was changed from deuterium to DT and tritium. Increased edge pedestal is found in ICRH discharges with -90° phasing resulting from the significantly broader fast-ion pressure profile due to the wave induced particle drift outwards [30].

In Fig. 3 and 4, we have assumed that the transition to H-mode occurs when type III or transition ELMs appear suddenly as the input power is ramped up. At this time the energy confinement makes a break from the L-mode and reaches the H-mode value and ELMs transform to Type I ELMs. As shown in Ref. [17], the frequency of Type III ELMs decreases whereas for type I ELMs increases with power. As an illustration of this dependence, in Fig. 11, we plot the ELM frequency as a function of power for NBI heated discharges at plasma currents and fields indicated in the figure for plasmas in hydrogen and, 100:0 and 10:90 D:T mixtures. We also note that the frequency of type I ELMs is lower with increasing isotope mass. In the case of hydrogen plasmas, the available power at this field was not sufficiently high for the establishment of type I ELMs. Nevertheless, trends in the frequency of ELMs with isotope mass is maintained. Note that clear type I ELMs in hydrogen plasmas have been obtained in JET at the lower field of 1T.

FIG. 11. ELM frequency is plotted as a function of NBI power in JET discharges with three different hydrogenic species: $H° \rightarrow H$, $D° \rightarrow D$ and $T° \rightarrow D:T$ (10:90%). Initial decrease in frequency with power is indicative of type III ELMs which then transform to type I ELMs when the frequency increases with power. In the hydrogen case, available power was not high enough (beyond the threshold value) to show clear type I ELMs.

A comparison of ELMs with ICRH and NBI has been done previously [31]. It is found that ELMs produced by ICRH have higher frequency and lower amplitude. At a given power input, the repetition rate and amplitude of ELMs is relatively less steady as compared to NBI but the energy confinement is about the same in the two cases. It is also found that power deposited on divertor tiles per ELM is smaller by a factor 2-5 as compared to beams. Here, we present results of ELM behaviour on the isotope mass (see Fig. 12). In both NBI and ICRH cases, the ELM frequency decreases with isotope mass and as mentioned above the ELM frequency is higher in the ICRH case by a factor of about 10-12 as shown.

As mentioned, the ELM frequency in the case of ICRH is not steady (estimated at an interval of every 100 ms) during the entire discharge and the variation is shown by the shaded
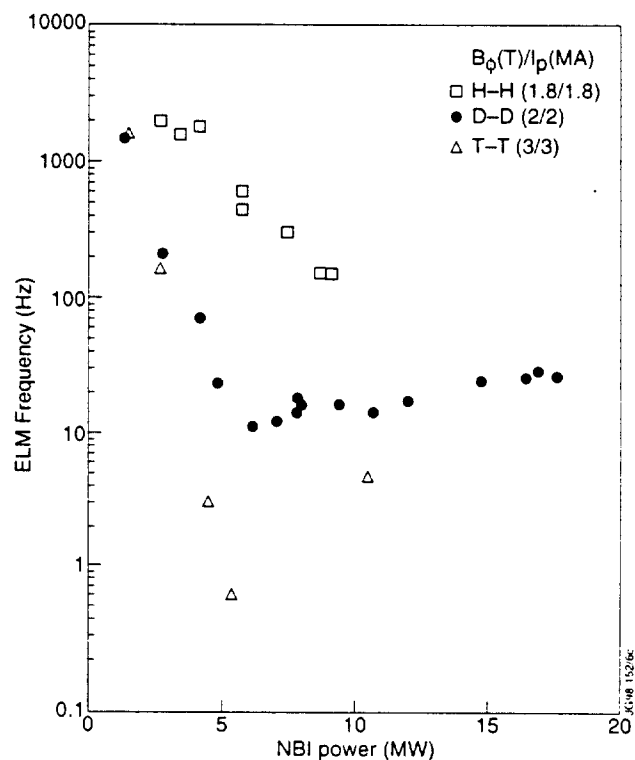
13

area in Fig. 12. This variation is in part due to the variation of parameters such as plasma density. The marked symbols in the three comparison shots represent the frequency measured when the density was equal.
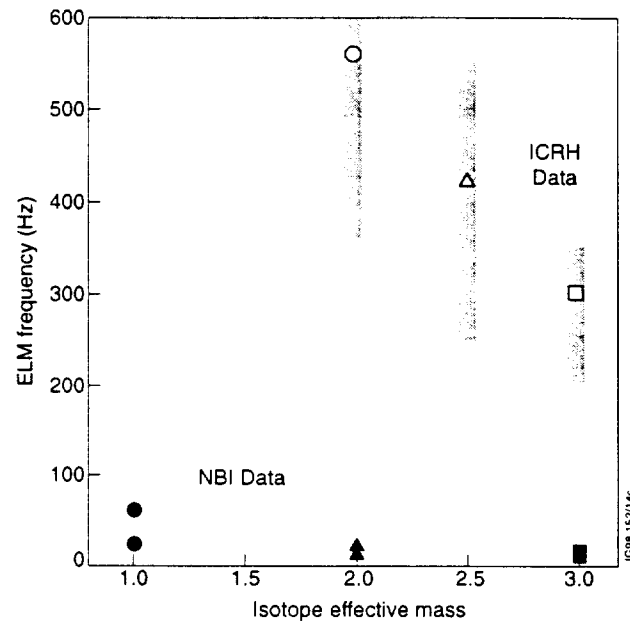

FIG. 12. ELM frequency is plotted as a function of isotopic mass of JET plasma in experiments carried out in different gas mixtures: hydrogen, deuterium, 50:50 D:T and 10:90 DT both in ICRH and NBI heated discharges. ELM frequency was not steady in ICRH discharges and the variation is represented by the shaded area.

7. TRACE TRITIUM PARTICLE TRANSPORT.

A knowledge of particle transport properties of a confined plasma is important in the design of ITER for the fueling requirements as well as for the plasma density control and the control of fusion power. While the electron transport or electron density profiles are easily measured in tokamaks, hydrogenic ion density profiles are difficult to measure directly except possibly via charge exchange enhanced atomic spectroscopy [32] of impurity ions. However, from trace tritium experiments in which 1-2% of tritium is puffed into ITER-relevant (see above) steady-state ELMy H-mode deuterium discharges, information on tritium transport can be inferred by the time evolution of the radial profile of 14 MeV DT neutrons [33-35]. Trace tritium experiments have also been carried out in discharges close to the Greenwald density limit where the particle confinement time is poorer [36].

The neutron profile monitor has been absolutely calibrated to provide line integral neutron yield. A 1 _ -D transport model [36] with diffusive and convective terms as well as a dynamic recycling model which describes the response of the wall to changes in the isotopic composition is used. The beam-thermal and thermal-thermal reactivities are also modeled. A least-square fit of parameters of the model to chordal neutron data together with a knowledge of the error bars on the signal permits the derivation of the transport coefficients.

14

Using the above procedure, in Fig. 13, we show profiles of tritium diffusion coefficient (D) in L-mode and H-mode discharges. Tritium was puffed in these deuterium discharges which were similar to the ρ^*-scaling discharges discussed above having ITER shape, q, β and v^*. The discharges used in L-mode were at B_ϕ/I_P of 2T/2MA and 3T/3MA heated with 2 and 3MW of NBI power respectively whereas in H-mode, 1T/1MA, 2T/2MA and 3T/3MA discharges heated by 5.8, 9.5 and 14 MW of NBI power respectively were used. Bohm and gyro-Bohm scalings of D are proportional to T_i/B_ϕ and $T_i^{3/2}/B_\phi^2$ respectively where T_i is the ion temperature. The measured values of D in L-mode discharges is close to 1 m^2/s both for 2 and 3T discharges. Normalizing to the 2T discharge, the expected band of values of D of the 3T discharge based on Bohm and gyro-Bohm scalings are shown in Fig. 13 (a). The uncertainty in T_i measurements is reflected in the shaded areas shown. The data in L-mode is slightly closer to the Bohm value, but the uncertainties in the measurement of T_i and D do not allow us to rule out one or the other. However, in H-mode discharges, the observed strong variation of D with B_ϕ for r/a<0.75 indicates a marked gyro-Bohm character in the core region. In this case, normalizing to the 1T discharge, the expected band of values of D of the 2 and 3T discharges are as shown in Fig. 13 (b). For the edge region (0.75 < r/a < 0.95), D does not depend on B_ϕ, and points to Bohm scaling but again with a large uncertainty. Thus we note that in H-mode, both the energy and particle diffusivities have a gyro-Bohm character in the core whereas in the edge-region, no definite conclusions can be reached due to large uncertainties in the measurements.
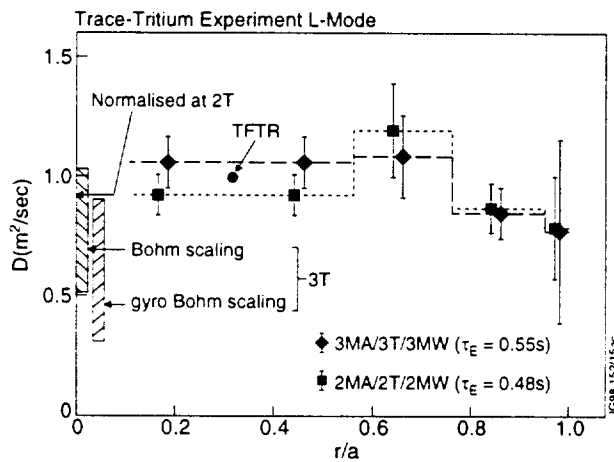

FIG. 13 (a). Profile of particle diffusivity (D) derived from JET trace tritium ITER similarity L-mode plasmas in deuterium at 2T/2MA and 3T/3MA. Normalised to 2T data, the expected band of values for Bohm and gyro-Bohm scalings for 3T are also shown. The shaded bands represent the uncertainty in T_i measurements.
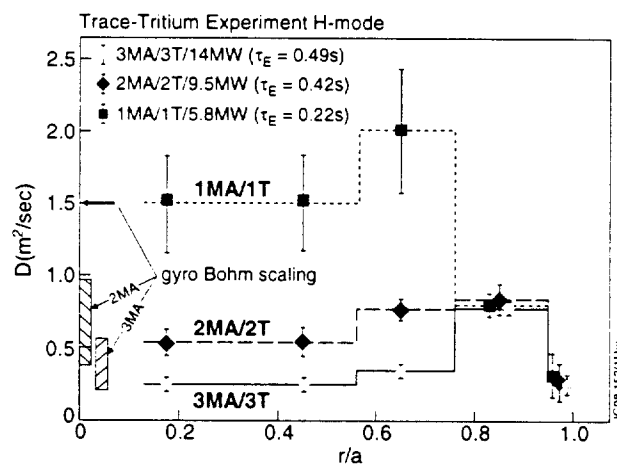
FIG. 13 (b). Profile of particle diffusivity (D) derived from JET trace tritium ITER similarity H-mode plasmas in deuterium at 1T/1MA, 2T/2MA and 3T/3MA. Normalized to 1T, the expected band of values for gyro-Bohm scaling for 2 and 3T are also shown. The shaded bands represent the uncertainty in T_i measurements.

8. H-MODE AND L-MODE DENSITY LIMITS

The density limit in tokamaks fueled with gas puffing and auxiliary heating is often represented by the empirical Greenwald limit [37] $n_{GW}(10^{20}m^{-3}) = I_p(MA)/\pi a^2(m^2)$. For achieving the rated fusion power in ITER (1.5 GW), it has to be operated above n_{GW} in ignited regimes or at about n_{GW} in the driven mode. Thus it is important to understand the underlying physics of density limits in tokamaks and find ways to increase the central density without degrading the confinement.
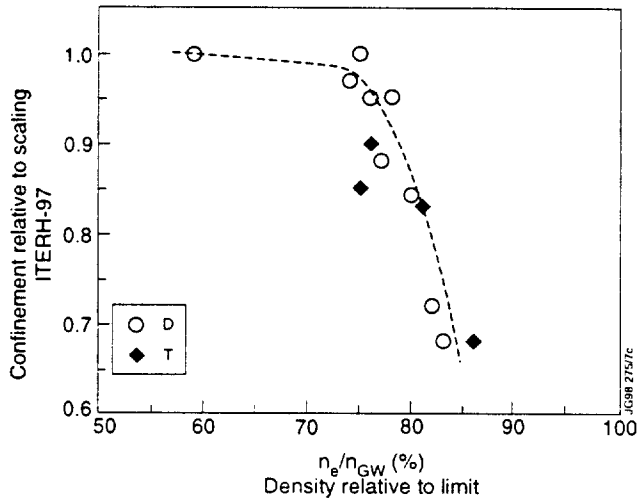

FIG. 14. *Thermal energy confinement time normalized to ITERH-93P scaling is plotted against plasma density normalized to Greenwald density limit (n_{GW}) [36] in JET discharges made in 100:0 and 10:90 D:T gas mixtures.*

A routine observation in JET is that at a given input power, increasing the plasma density in ELMy H-modes by increased gas fuelling leads to a degradation in global particle confinement. At some point, this loss outweighs the additional gas fuelled particle source and an effective density satuaration is reached [38] without undergoing a disruption. As the density limit is approached, the thermal energy ELMy H-mode confinement time also degrades as compared to the ITERH97y value. This is illustrated in Fig. 14, which shows data on a comparison of deuterium and tritium gas puffed discharges heated with 11-12 of NBI power at 2.6T/2.6MA. We note that the ELMy H-mode thermal energy confinement time both in deuterium and tritium plasmas decreases significantly when the plasma density exceeds 0.75 of the Greenwald (n_{GW}) limit. Both in deuterium and tritium discharges, the maximum density achieved is $0.85n_{GW}$. The degradation in energy confinement with additional gas fuelling is most probably related to the lowering of the edge pressure pedestal. As the gas fuelling is made more strong, the region of confinement degradation starts to expand from the edge to the core [38]. Such a degradation could be avoided by deep fuelling by pellet injection.

The ultimate density limit in L-mode discharges is due to a thermal instability originating in the divertor region which terminates in a disruption. The 2-D EDGE2D/NIMBUS code [39] simulations predict this limit to decrease with increasing hydrogenic isotope mass due to a smaller penetration range of hydrogen neutrals. L-mode experiments have been conducted in hydrogen, deuterium and tritium without additional heating to benchmark the code in this respect. The density limit is indeed found to decrease with increasing isotope mass as shown in Fig. 15. In this figure, the degree of detachment (DoD), as defined in Ref. 40, of the inner divertor leg is

plotted as a function of the central line averaged density. In all three pulses, the discharges disrupts when the DoD value reaches about 100. The vertical broken lines drawn are the code predictions [39] which have been normalized to the deuterium case for comparison as the code produced output of upstream separatrix density is not experimentally measured [41]. Similar results are obtained on the outer divertor leg [41] with detachment occurring at about the same density. With respect to this mass dependence, it is believed that at constant energy, the reduced ionization length with heavier mass leads to more recycling and effectively to a more closed divertor. This in turn leads to a higher degree of detachment at a given upstream (or core) density and thus to a lower ultimate achievable density before disruption with heavier isotope mass.
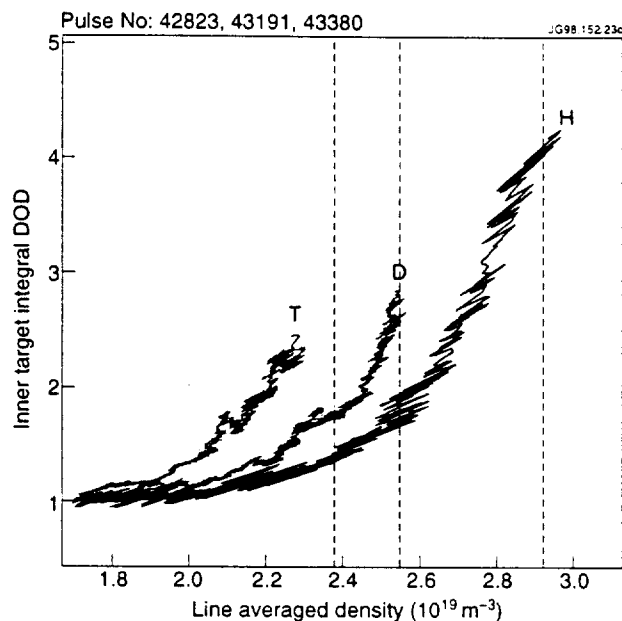

FIG. 15. *The inner target degree of detachment (DoD) leading up to the L-mode density limit is plotted as a function of line averaged plasma density in three discharges made in hydrogen, deuterium and tritium. The vertical lines are EDGE2D/NIMBUS code predictions [39] normalized to deuterium for the L-mode density limits in these discharges.*

9. ICRH EXPERIMENTS IN D/T PLASMAS

For ITER, second harmonic heating of tritium ($2\omega_{CT}$) and deuterium minority heating at fundamental cyclotron frequency (ω_{CD}) are the two Fast-wave reference heating scenarios. Subsequent to the ICRH DT experiments performed at $2\omega_{CT}$ in circular limiter plasmas in TFTR [42], JET has carried out ICRH experiments in the ITER-relevant DT scenarios and in ITER-like configuration [43] with $0\pi0\pi$-phasing of the 4-strap ICRH antennae. The reference ITER antenna design also uses 4-strap antenna arrays. ICRH experiments in DT plasmas in JET have demonstrated strong bulk ion heating in the $2\omega_{CT}$ scheme by the addition of He3-minority ions. Also, strong single-pass damping (more than 90%) experiments in JET with hydrogen minority in tritium [44] plasmas are akin to those that will prevail in ITER. Results of D-minority heating in tritium with the achievement of steady-state $Q\approx0.22$ with ICRH alone have already been presented in Section 5.

Second harmonic heating of tritium ($2\omega_{CT}$) experiments were carried out using freshly reprocessed tritium to minimize the content of He^3 in the plasma due to radio-active decay of tritium so that He3 minority ion absorption is avoided. Time traces of a $2\omega_{CT}$-heated discharge at 8 MW power level are shown in Fig. 16. Since this heating scheme utilizes a finite Larmor radius effect, the heated population absorbs the power predominantly producing a large tail.
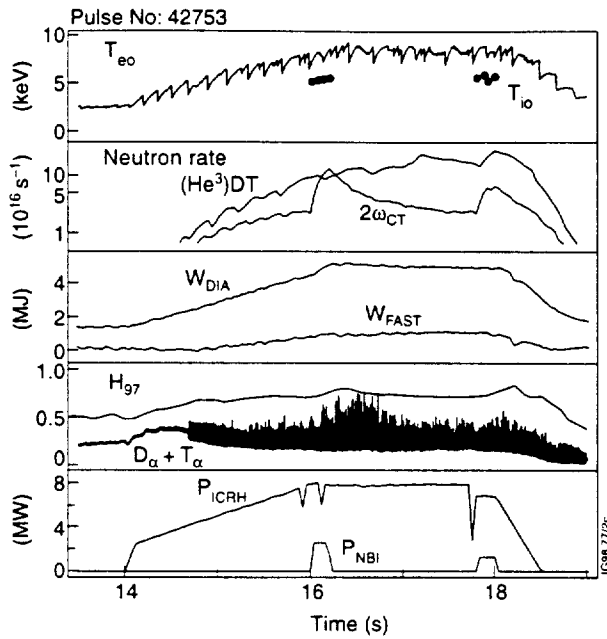
FIG. 16. *Time traces of a second harmonic ($2\omega_{CT}$) ICRF heating of tritium in a 43:57 D:T plasma at 3.7T/3.3 MA. Here, W_{FAST} refers to the fast ion energy content of the plasma. The neutron yield (note the logrithmic scale) is much smaller compared to the He3-minority heating which produced stronger ion heating as shown in Fig. 18.*

This was decreased by operating at high plasma density (5×10^{19}m^{-3}) but the tail could not be lowered enough to achieve dominant ion heating. Nevertheless, the performance of the discharge was in line with expectations. The central electron and ion temperatures obtained are 8 and 6 keV respectively. Due to weaker single pass damping, the power deposition profile is broader resulting in a lower ITERH97 factor of 0.7. ELMs appear to be more like grassy or type III ELMs and their frequency is high. In this discharge, the fast ion energy (W_{FAST}) is about 20% of the diamagnetic stored energy (W_{DIA}). The full potential of the $2\omega_{CT}$ heating scheme is expected to be achieved in ITER where the plasma density would be higher (1×10^{20}m^{-3}) resulting in lower tails and dominant bulk ion heating. Nevertheless, if 5-10% of He3 is injected into the above $2\omega_{CT}$-heating JET discharge, (see below) a strong ion heating is observed and the neutron yield is improved significantly.

Puffing a small amount (>2%) of He^3 (in addition to the He^3 present due to radio-active decay) improves significantly the wave absorption and the energy confinement [44]. In such a case, minority (He^3) ion absorption dominates (as in (H)-D plasma) and a significant He^3 tail is produced. By adding He^3 to a level of 5-10 %, He^3-tail can be sufficiently lowered to produce strong ion heating. Time traces of such a discharge are shown in Fig. 17 (a) where $T_{i0} \approx 13$ keV is achieved by ICRH alone. He^3-minority heats ions efficiently as the averaged energy of the He^3-tail is smaller and the critical energy for equal power transfer to electrons and ions ($P_e = P_i$) is 3 times higher than that of H. Central electron and ion temperatures in this discharge are roughly equal. Also, the ITERH97 factor is higher, nearly unity in this case. Expansion of the D_α-signal (box 3) shows that in this case discrete ELMs occur and their frequency is lower than that in the $2\omega_{CT}$ case shown in Fig. 17. This is consistent with the higher energy density of fast ions in the edge found by the PION [28] code calculations in the case of He3 minority heating. Electron and ion temperature profiles given in Fig. 17(b) show that the T_i-profile is more peaked than that of T_e. This is consistent with lower energy of the He^3-tail (smaller fast-ion orbits) power transfer to background species in a narrow region combined with the effect of broader direct electron absorption by electron transit time magnetic pumping (e-TTMP).
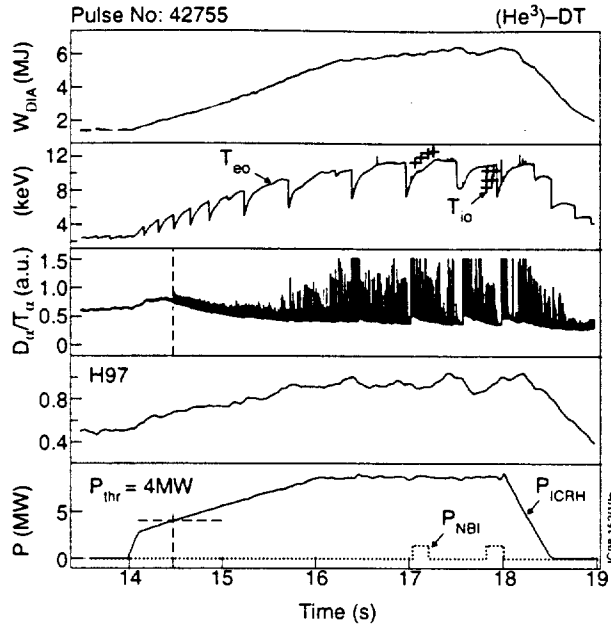
18

FIG. 17 (a). Time traces of a He3-minority ICRF heating of a 45:55 D:T plasma with about 10% of He3 added. Other parameters are $B_\varphi=3.7T$, $I_P=3.3MA$, $f=37.2MHz$, and $n_{e0}=3.2x10^{19}m^{-3}$. Central electron and ion temperatures are 12 and 13 keV respectively. The ITERH97-Py factor is close to unity.

FIG. 17 (b). Electron and ion temperature profiles in the He3-minority ICRF heating DT discharge presented in Fig. 18 (a). T_e is measured by electron cyclotron emission (ECE) and T_i by charge exchange recombination spectroscopy (CX)

10. EXTRAPOLATION TO ITER

The energy confinement in ITER DT plasmas can be predicted by using the JET data obtained in ~50:50 DT plasmas thereby avoiding the uncertainties of the isotope mass scaling. The experimentally obtained thermal energy confinement time in such plasmas is plotted versus the ITERH97-P scaling formula, in Fig. 18, in dimensionless form with an isotope mass value of 2.5. This data is then compared with the ITER requirement for ignition at appropriate parameters in ITER simulations. We note that the JET data extends over more than one order of magnitude in normalized confinement time and that a similar gap exists between the top of the JET data and ITER. However, the extrapolated confinement time is in line with the ITER expectation of 6s required for ignition. There is of course a large uncertainty in extrapolat-

FIG. 18. Thermal energy confinement time data of DT shots extracted from Fig. 7 is plotted in normalized form against the normalized ITERH-97Py scaling together with the value expected for ITER. Here, B is the toroidal field which is proportional to cyclotron frequency and used for normalization purposes without taking account of charge and mass. The ITER expected value of confinement in DT plasmas is in line with that extrapolated from JET DT data.

19

ing the confinement time using the JET data alone since the high current data does not quite have the β required for ITER due to a lack of input power in these shots.

Table 1: Extrapolated ITER values from JET data based on scaled stored energy

Parameters	Units	JET Pulses			ITER
		42756	42982	42983	Basic operation
Major radius, R	m	2.91	2.90	2.89	8.14
Minor radius, a	m	0.93	0.94	0.96	2.80
Toroidal magnetic field, B	T	1.95	3.9	3.46	5.68
Plasma current, I_p	MA	1.97	3.8	4.46	21 (24)
Safety factor at r/a=0.95, $q_{\psi,95}$		3.4	3.5	2.76	~3.2(2.8)
Stored energy, W_s	MJ	5.2	10.3	13.8	1100
Normalized pressure, β_N		2.4	1.3	1.7	2.2
Averaged density, $<n_e>$ (10^{19})	m^{-3}	5.0	6.5	8.0	9.8
Power input, P_{in}	MW	17.3	24.6	24.4	182
Extrapolated ITER values					
Scaled energy, $W_s \propto B^2 a^3$	MJ	1204	586	922	
Scaled Fusion power, P_{FUS} (see text)	MW	1797	426	1053	
Alpha power, P_α	MW	359	85	211	
Scaled $<n_e> \propto B^{4/3} a^{1/3}$ (10^{19})	m^{-3}	14.4	7.4	10.7	
Bremsstalung power, P_{Brems} (see text)	MW	219	57	123	
$P_\alpha - P_{Brems}$	MW	140	28	88	
Power to support stored energy					
(a) Gyro-Bohm scaling $P_{G-B} \propto B a^{1/2}$	MW	87	62	69	
(b) Bohm scaling $P_B \propto B^{5/3} a^{4/3}$	MW	447	197	232	
Fusion power Amplification					
(a) Q (Gyro-Bohm scaling)		∞	13	∞	
(b) Q (Bohm scaling)	m	5.8	2.5	7.3	

We have carried out a performance extrapolation to ITER based on specific JET D-T discharges in which the toroidal β and the collisionality ν^* is maintained in ITER. In the extrapolation, the horizontal minor radius is taken as the length scaling parameter since the aspect

ratio and plasma elongation in JET and ITER are only slightly different. A comparison of the parameters of three (2T/2MA, 3.5T/4.5MA and 3.9T/3.8MA) high performance JET steady-state DT discharges with those used for basic operation of ITER is given in the upper half of Table 1. The value of β_N=2.4 for the 2MA discharge is slightly higher than the ITER value (β_N =2.2) whereas for the other two discharges it is lower than that for ITER. Extrapolated ITER values based on these discharges are listed in the lower half of the table. Dimensionless scaling constraints permit to extrapolate, for example, the stored energy for fixed β scales as

$$W_s \propto B^2 a^3 \tag{4}$$

where B is the toroidal field and a is the plasma minor radius. Scaled stored energy values thus obtained are shown in Table 1. Noting that the fusion power is proportional to the square of stored energy near the optimum ion temperature, we deduce the scaled fusion power output in ITER corresponding to each of the above JET discharge knowing from ITER calculations, 1100 MJ of stored energy would produce a fusion power output of 1500 MW. The power lost by Bremstrahlung is taken to be 118 MW from the ITER Final Design Report [45] and is scaled as $P_{Brems} \propto n_e^2 T_e^{1/2} \propto n_e^{3/2} W_s^{1/2}$ for these extrapolations. The input power needed to sustain the above stored energy is calculated based on gyro-Bohm and Bohm scaling of energy confine-ment time which scales as indicated in Table 1. At the end of the table, the predicted Q values are given for both the above gyro-Bohm and Bohm scalings. By looking at the parameters of the third discharge (42983), we note that ignition (Q=∞) can be achieved with relatively low β_N=1.7 and low $q_{\psi95}$, though at a somewhat reduced power output of 1274 MW. Extrapolation based on this particular shot shows that reasonable value of Q~7 can be obtained even with the very pessimistic assumption of Bohm transport throughout the plasma. Note that, in principle, one should subtract the power radiated from the core (Bremsstrahlung + impurity) from the power input in the JET pulses to calculate the extrapolated values of Q for ITER. This has not been done here so the calculations presented in Table 1 are conservative (lower by 20%) estimates of Q.

11. DISCUSSION AND CONCLUSIONS

We have presented, in this paper, an overview of JET results of ITER physics experiments carried out in D/T plasmas in which the D:T mixture was varied from 0:100 to 10:90. Emphasis was placed to bring out the dependence of isotope mass on important quantities such as H-mode threshold power, energy confinement, ELMs, edge pedestal and density limits in tokamak plasmas. To extend the mass range, results of dedicated experiments carried out in hydrogen after the DTE1 campaign have also been included. Experiments were carried out in plasmas with ITER geometry and q and special effort was made to match the key physics dimensionless parameters such as β and v^* to their ITER value. The other important parameter ρ^* was varied to determine

the ρ^*-scaling of confinement and then extrapolate to ITER. The electron and ion temperatures were very close to each other as expected in ITER. Results of experiments conducted to validate the ICRH reference scenarios in ITER have also been presented.

These results have the following important implications for ITER:

(i) From experiments in H, D and T-plasmas, a clear reduction in H-mode threshold power is seen as isotope mass is increased. A regression analysis of JET data is consistent with an inverse mass dependence of threshold power. This result has a favourable consequence of a reduction of about 25% the power requirement in ITER (as compared to the earlier projections) to reach the high confinement regime and considerably widens the ITER route to ignition. However, the uncertainties in power exponents in Eq. 1 and 2, especially that of density, are still significant and points towards additional physics not included in the present scaling formulation. Note also, that the above results of power threshold are independent of heating method.

(ii) JET results show that the global energy confinement is practically independent of isotopic mass. The confinement in H-mode plasmas is considered to be composed of two parts: (a) the core which is governed by the physics form of gyro-Bohm transport ($\sim A^{-0.2}$) and (b) the ELMy edge in which the pedestal energy scales as $\sim A^{0.57 \pm 0.2}$. This leads to the result that the net effect of isotope mass on global energy confinement is negligible. This difference in mass scaling of the core and the edge emphasizes the importance of JET which is less dominated by plasma edge effects than smaller machines. In the final analysis, the unfavorable mass dependence, as compared to the earlier ITER projections, is compensated by the stronger density dependence found in the JET data. This is confirmed in Fig. 18 where the ITER confinement time required for ignition is in line with the JET DT data albeit following different power coefficients of density and isotope mass than the earlier scaling. Note that this assumes that ITER could be operated near the Greenwald density limit without a significant degradation of confinement (see below).

(iii) In both deuterium and tritium gas fueled ELMy H-mode plasmas, the thermal energy confinement decreases towards L-mode as the Greenwald empirical density limit is approached. The maximum density achieved in JET with a given plasma geometry is about $0.85n_{GW}$ both in deuterium and tritium. It will be essential to check, in future experiments with deep fueling injection, if this trend can be avoided. The L-mode density limit is found to decrease with increasing isotope mass in agreement with the 2-D code predictions.

(iv) High current, high power near steady-state discharges with ITER q and geometry in 50:50 DT plasmas achieved high performance with fusion power output of 4.1 MW and a $Q \approx 0.18$ in which type I ELMs are maintained throughout the discharge for more than 3.5 s. This lends strong support to the ITER mode of steady-state operation with type I ELMs assuming that the problem of target erosion during type I ELMs can be resolved satisfactorily by appropriate divertor design. Discharges heated with ICRF alone in D-minority scheme

produce a steady-state $Q \approx 0.22$ at an input power of 6MW where the neutrons were of non-thermal origin. Note that with ICRH both small ELMs and good confinement could be maintained simultaneously (see below).

(v)   The observed scaling of the edge pedestal energy ($\sim A^{0.57 \pm 0.2}$) is consistent with a model in which the edge pressure gradient saturates at the ballooning limit over a region of width that scales as the ion poloidal Larmor radius governed by the average fast-ion tail energy in the edge. This pedestal width scaling is different from the size scaling assumed in the ITER Final Design Report [46]. This would have important consequences for the edge pedestal temperature in ITER and based on our results it should be calculated with the slowing down energy spectra of α-particles at the edge. The steady-state total stored energy for a given input power both in ICRH and NBI heated discharges is found to be the same. However, the edge electron pressure pedestal (p_e) with ICRH is smaller by a factor of about 4 than in the NBI case. This is due to the fact that ICRH power deposition profiles are much more peaked than those of NBI as the latter leaves a substantial foot-print resulting in a broader power deposition profile, particularly as the H-mode develops and the density increases.

(vi) The ELM frequency is found to decrease with isotope mass both in ICRH and NBI discharges. However, the frequency in the case of ICRH is about 8-10 times higher than the NBI case. This has a favourable consequence for ITER concerning the peak heat load on the divertor plates which is smaller by a factor of 2-5 in the case of ICRH [31] where the edge pressure remains low.

(vii) The tritium transport experiments in H-mode indicate that for $r/a < 0.75$, the particle diffusivity exhibit gyro-Bohm scaling whereas for $0.75 < r/a < 0.95$, it points to the Bohm scaling with a large uncertainity.

(viii) ITER reference scenarios (tritium second harmonic and deuterium-minority heating) in DT plasmas have been successfully tested. A small concentration of He3 added in the former scheme produced strong bulk ion heating ($T_{i0} \approx 13$ keV) due to improved power localization and lower He3 tail energies. A good agreement is found between PION code predictions and experimental results. The present ICRH results obtained on JET constitute a firm experimental basis for the application of ICRH on ITER. In particular, the significant bulk ion heating will facilitate an easier access to the H-mode regime and could also provide higher Q in the driven mode of ITER.

(ix) An extrapolation of the performance of steady-state JET DT discharges to ITER has been made based on stored energy achieved and assuming gyro-Bohm or Bohm scaling of the energy confinement. Using the former scaling and under assumptions listed in Section 9, ignition ($Q = \infty$) in ITER with a fusion power output of 1.05 GW is predicted based on the JET discharge 42983 featuring a $\beta_N = 1.7$ only. For the same discharge, a Q=7.3 can be achieved when the pessimistic Bohm scaling is used.

In conclusion, a combination of JET features such as large-scale plasma, flexible heating and current-drive systems, ITER-like divertor configuration with C and Be for plasma-facing components and operation in DT plasmas have made JET a unique device for making the most relevant contributions to the ITER modes of operation. This is clearly borne out from the results presented in the paper which have provided a new and more firm experimental base to consolidate the physics basis of ITER. Overall, the JET results obtained in DT plasmas are a welcome news for ITER.

Nevertheless, significant work remains to be done for ITER which will guide the future programme of JET culminating in a further campaign of DT experiments. Besides α-particle heating experiments, the most relevant future work in the ITER modes of operation includes:

(a)   A confinement database to be constructed with data near or above the Greenwald density limit, at lower q (~2.7) and at the ITER values of β_N. This will require systematic use of deep fuelling methods.

(b)   A clearer understanding of the physics of accessing the H-mode and, in particular, reducing the uncertainties in the power exponents of plasma parameters appearing in the H-mode threshold scaling (see Eq. 2) and developing a more physics based model.

(c)   A modification of the scaling laws of energy confinement based on the recognition of the fact that the dominant physics of the plasma core and edge are different.

(d)   An extension of the operation of the $2\omega_{CT}$-heating scheme to ITER-like densities together with the issues such as the effect of antenna phasing on the heating efficiency and ELM-resistant antenna-plasma matching techniques for maintaining good coupling during strong ELM activity.

ACKNOWLEDGEMENTS

REFERENCES

[1]   AYMAR, R., et al., ITER JOINT CENTRAL TEAM, HOME TEAMS, in Fusion Energy (Proc.16th Int. Conf. Montreal, 1996), vol.1, IAEA, Vienna (1997) 3.

[2]   JET TEAM, Annual Report 1996, JET Joint Undertaking, Abingdon (UK).

[3]   JET TEAM, Nucl. Fusion 38 (1998) .... (companion paper)

[4]   LASSER, R. et al., Proc. Workshop on Tritium Experiments in Large Tokamaks : Applications to ITER, Princeton Plasma Physics Laboratory, March 1998.

[5]   KEILHACKER, M. J., JET TEAM, in Plasma Physics and Controlled Fusion Research (Proc.14th Int. Conf. Wurzburg, 1992), vol.1, IAEA, Vienna (1992) 15.

[6]   JACQUINOT, J., JET TEAM, Fusion Engineering and Design 30 (1995)67.

[7]   JET TEAM, Progress Report 1996, JET Joint Undertaking, Abingdon (UK).

[8]   KAYE, A. et al., Fusion Engineering and Design 24 (1994) 1.

[9]   STORK, D., Fusion Engineering and Design, 14 (1991) 111.

[10]   JET TEAM (Presented by J. JACQUINOT), Plasma Physics Controlled Fusion 33(1991)1657.

[11]   STOTT, P., in Diagnostics for Fusion Reactor conditions (Proc. International School of Plasma Physics, 1982), vol. 1, Commission of the European Communities, Brussels, 1982, p.3.

[12]   ORLINSKIJ, D.V. , MAGYAR, G., Nucl. Fusion 28 (1988) 611.

[13]   MORGAN, P. D. et al., Report JET-R(97)08, JET Joint Undertaking, Abingdon (UK) 1997.

[14]   CORDEY, J. G. et al., Report JET-P(94)66, JET Joint Undertaking, Abingdon (UK).

[15]   H-MODE DATABASE WORKING GROUP, in Controlled Fusion and Plasma Physics (Proc. 21st Eur. Conf, Montpellier, 1994), vol.18B, Part I, European Physical Society, Geneva (1994) 334.

[16]   H-MODE DATABASE WORKING GROUP (presented by T. TIKIZUKA), in Fusion Energy (Proc.16th Int. Conf. Montreal, 1996), vol.2, IAEA, Vienna (1997) 795.

[17]   ZOHM, H., Plasma Physics Controlled Fusion 38 (1996) 105.

[18]   RIGHI, E. et al., to be submitted for publication in Nucl. Fusion special issue.

[19]   ITER CONFINEMENT DATABASE AND MODELLING WORKING GROUP (Presented by J.G. CORDEY), Plasma Physics Controlled Fusion 39 supplement 12B (1997) B115.

[20]   H-MODE DATABASE WORKING GROUP, in Controlled Fusion and Plasma Physics (Proc. 20th Eur. Conf, Lisbon, 1993), vol.17C, Part I, European Physical Society, Geneva (1993) 15.

[21]   PETTY, C.C., LUCE, T.C., in Controlled Fusion and Plasma Physics (Proc. 24th Eur. Conf, Berchtesgaden, 1997), vol.21A, Part III, European Physical Society, Geneva (1997) 1085.

[22]   JACQUINOT, J., JET TEAM, to be published in Nucl Fusion (Alpha-5).

[23]   CORDEY, J.G. et al., to be submitted for publication in Nucl. Fusion special issue.

[24]   KAYE, S. M., ITER L-MODE CONFINEMENT DATABASE WORKING GROUP, Nucl. Fusion 37 (1997) 1303.

[25]   McGUIRE, K. M. et al., in Fusion Energy (Proc.16th Int. Conf. Montreal, 1996), vol.1, IAEA, Vienna (1997) 19.

[26]   HORTON, L. et al., to be submitted for publication in Nucl. Fusion special issue.

[27]   START, D.F.H. et al., Report JET-P(97)59, JET Joint Undertaking, Abingdon (UK), 1997, submitted to Phys. Rev. Lett.

[28] ERIKSSON, L-G. et al, to be submitted for publication in Nucl. Fusion special issue.

[29] BHATNAGAR, V.P., LINGERTAT, J. et al, to be submitted for publication in Nucl. Fusion special issue.

[30] ERIKSSON, L-G. et al, submitted to Phys Rev. Letters, see also Report JET-P(98)07, JET Joint Undertaking, Abingdon (UK)

[31] BHATNAGAR, V.P. et al., in Controlled Fusion and Plasma Physics (Proc. 24th Eur. Conf, Berchtesgaden, 1997), vol.21A, Part I, European Physical Society, Geneva (1997) 77.

[32] FONCK, R.J. et al., Report PPPL-1908, Princeton Plasma Physics Laboratory, Princeton (USA) 1982.

[33] STRACHAN, J., et al., J. Vac. Sci. Technol.. A, 1 (1983) 811.

[34] MARCUS, F.B., et al, Nucl. Fusion 33 (1993) 1325.

[35] EFTHIMION, P.C., et al., Phys. Rev. Lett. 75 (1995) 85.

[36] ZASTROW, K.D., et al., to be submitted for publication in Nucl. Fusion special issue.

[37] GREENWALD, M., et al., Nucl Fusion 28 (1988) 2199.

[38] SAIBENE, G., et al., to be submitted for publication in Nucl. Fusion special issue.

[39] SIMONINI, R., et al., Plasma Physics and Controlled Fusion, 34 (1994) 368.

[40] LOARTE, A., et al., Nucl Fusion 38 (1998) 331.

[41] MAGGI, C., et al., to be submitted for publication in Nucl. Fusion special issue.

[42] WILSON, J.R. et al., Phys Rev. Lett. 75 (1995) 842.

[43] START, D.F.H., et al., to be submitted for publication in Nucl. Fusion special issue.

[44] BHATNAGAR, V.P. et al., in RF Heating and Current Drive of Fusion Devices (Proc. 2nd Europhysics Topical Conf, Brussels, 1998), vol.22A, European Physical Society, Geneva (1998) 29.

[45] JET TEAM (Presented by JACQUINOT, J.), in Controlled Fusion and Plasma Physics (Proc. 24th Eur. Conf, Berchtesgaden, 1997), vol.21A, Part IV, European Physical Society, Geneva (1997) 1865.

[46] ITER CENTRAL TEAM, Final Design Report, International Thermonuclear Experimental Reactor Engineering Design Activity, San Diego Joint Work Site, La Jolla, California, 1997 (unpublished).